Journal of Advanced Ceramics
2021, **10**(3): 482–492
https://doi.org/10.1007/s40145-020-0450-1
ISSN 2226-4108
CN 10-1154/TQ

Research Article

Enhanced electrocaloric effect at room temperature in Mn^{2+} doped lead-free $(BaSr)TiO_3$ ceramics via a direct measurement

Xiang NIU[a,†], Xiaodong JIAN[a,b,†], Xianyi CHEN[a,b], Haoxuan LI[a], Wei LIANG[a], Yingbang YAO[a,b], Tao TAO[a,b], Bo LIANG[a,b], Sheng-Guo LU[a,b,*]

[a]*Guangdong Provincial Research Center on Smart Materials and Energy Conversion Devices, Guangdong Provincial Key Laboratory of Functional Soft Condensed Matter, School of Materials and Energy, Guangdong University of Technology, Guangzhou 510006, China*
[b]*Dongguan South China Design Innovation Institute, Dongguan 523808, China*

Received: August 25, 2020; Revised: November 24, 2020; Accepted: December 24, 2020

Abstract: $(Ba_{1-x}Sr_x)(Mn_yTi_{1-y})O_3$ (BSMT) ceramics with x = 35, 40 mol% and y = 0, 0.1, 0.2, 0.3, 0.4, 0.5 mol% were prepared using a conventional solid-state reaction approach. The dielectric and ferroelectric properties were characterized using impedance analysis and polarization–electric field (P–E) hysteresis loop measurements, respectively. The adiabatic temperature drop was directly measured using a thermocouple when the applied electric field was removed. The results indicate that high permittivity and low dielectric losses were obtained by doping 0.1–0.4 mol% of manganese ions in $(BaSr)TiO_3$ (BST) specimens. A maximum electrocaloric effect (ECE) of 2.75 K in temperature change with electrocaloric strength of 0.55 K·(MV/m)$^{-1}$ was directly obtained at ~21 ℃ and 50 kV/cm in $Ba_{0.6}Sr_{0.4}Mn_{0.001}Ti_{0.999}O_3$ sample, offering a promising ECE material for practical refrigeration devices working at room temperature.

Keywords: barium strontium titanate ceramics; permittivity; dielectric loss; electrocaloric effect; electrocaloric strength

1 Introduction

With the fast increasing numbers of transistors in modern integrated circuits entry, thermal accumulation has become one of the crucial factors for chip damage, which causes not only the high electrical consumption, but also the thermal impact on the stability of the electronic components [1,2]. Thus, an urgent demand on the development of novel on-chip cooling modulus for miniaturized electronic devices raises. Recently, numerous refrigeration technologies have been extensively investigated, including magnetocaloric effect refrigeration, elastocaloric effect refrigeration, electrocaloric effect (ECE) refrigeration, and thermoelectric cooling refrigeration. Among all these approaches, the ECE has been considered as a more attractive means owing to its high energy conversion efficiency (more than 60% of Carnot cycle), flexibility for customized probe design, easy-miniaturization, and environmentally-friendly features. ECE refrigeration has been regarded as a prospective candidate for new generation of refrigeration approach to replace the

† Xiang Niu and Xiaodong Jian contributed equally to this work.
* Corresponding author.
E-mail: sglu@gdut.edu.cn

traditional vapor-compression technology.

The ECE occurred in polar materials and induced by the variation of electric field. It is denoted by the adiabatic temperature change (ΔT) or isothermal entropy change when an external electric field was applied or removed in certain polar materials [3–5]. The earliest reported regarding ECE can be traced back to the report of a finite temperature change (about 0.0036 K) in Rochelle salt by Wiseman and Kuebler in 1963 [6]. However, much effort has been devoted to ECE recently since the giant ECE responses have been reported for $Pb(ZrTi)O_3$ thin films in 2006 [7] and poly(vinylidene fluoride-trifluoroethylene) [P(VDF–TrFE)] copolymers and poly(vinylidene fluoride–trifluoroethylene–chloro-fluoroethylene) [P(VDF–TrFE–CFE)] terpolymers in 2008 [8]. Regarding the thermodynamic theory, the isothermal entropy change ΔS of certain ECE materials can be estimated by

$$\Delta S = -\frac{1}{2}\beta \Delta P^2 \tag{1}$$

where β is the phenomenological coefficient of P^2 in the Gibbs free energy expression of the Landau theory, and P represents the polarization contributed by dipoles' switching in ferroelectric phase, which implies that a large ECE is generally associated with a large polarization change. In other words, a large ECE material should presents a large polarization variation under an electrical stimulation. As discussed above, ferroelectrics, e.g., polyvinylidene fluoride (PVDF)-based polymers, ferroelectric (antiferroelectric) ceramics, single crystals, thin films, and liquid crystals, have been considered as the promising option to meet such requirements due to not only its intrinsic large spontaneous polarization, but also the large ferro- to para-electric phase transition heat. Among them, thin films with at least 10 times higher breakdown electric field than bulk ceramic counterparts, which show large ECE responses. Lu *et al*. [9] reported a giant ΔT = 40 K found in $(PbLa)(ZrTi)O_3$ (PLZT) (8/65/35 mol%) thin film at 318 K and 1200 kV/cm. Thin film materials, however, are not self-standing, require an indispensable substrate to support their mechanical structure, which are redundant parts for the development of cooling devices besides their extremely weak thermal mass led to a small cooling power. Ferroelectric polymers have also been drawn attention because of their large ECE response introduced by the high breakdown electric field of over 10,000 kV/cm. For instances, Lu *et al*. [9] reported a large ΔT = 20 K at 306 K and 1600 kV/cm in high-energy electron irradiated P(VDF–TrFE) (68/32 mol%) copolymers. Unfortunately, the low thermal conductivity (~0.2 W/(m·K)) makes polymer materials a poor thermal transporter while pursuing the thermal exchange between the frigerant and the thermal switch. Compared with two options above, bulk ceramics, e.g., in 2011, Rožič *et al*. [10] reported a large $\Delta T \approx 2$ K for PLZT (8/65/35 mol%) bulk ceramics at ~410 K, and a $\Delta T > 2.5$ K for $0.7Pb(Mg_{1/3}Nb_{2/3})O_3$–$0.3PbTiO_3$ (PMN–0.3PT) bulk ceramics at ~410 K with 88 and 90 kV/cm of external fields, respectively, and other numerous ferroelectric bulk materials with good electrocaloric properties have been reported [11–13].

Taking both the environmental friendliness characteristic and large ECE response into consideration, lead-free $BaTiO_3$ (BTO)-based ferroelectric ceramics with a perovskite structure is a promising ECE candidate, due to their first-order phase transition as well. However, for ECE in ferroelectrics, the large polarization change and ECE performance always take place near the ferroelectric–paraelectric phase transition temperature (Curie temperature, T_C), while the T_C of BTO is about 120 ℃, which is far from room temperature. Moreover, as a first-order phase transition ferroelectric, the desired ECE performance only occurs within a narrow temperature range. More critically, the dielectric loss due to the oxygen vacancies generated at high temperatures during the sintering process is always an issue in mitigating the breakdown electric field. In this work, these issues will be addressed via ionic doping in both A- and B-site of perovskite structure [14–24]. Here, Sr^{2+} ions are used to shift the phase transition towards room temperature. Manganese ions are imported to compensate the oxygen vacancies to enhance the ECE properties and lower the dielectric losses. The Mn^{4+} ions will be reduced into Mn^{2+} in terms of attracting two electrons from the oxygen vacancy V_{O_2} during the sintering process at high temperatures, which will be oxidized into $V_{O_2}^{\bullet\bullet}$. Since the oxygen vacancies are attracted by the Mn^{2+} ions, the movable oxygen vacancies will be greatly mitigated, then the loss tangent will be declined [25].

2 Experimental

2. 1 Sample preparation

$(Ba_{1-x}Sr_x)(Mn_yTi_{1-y})O_3$ (BSMT) ceramics with x = 35, 40 mol% and y = 0, 0.1, 0.2, 0.3, 0.4, 0.5 mol% were

prepared using a conventional solid-state reaction method. $BaCO_3$, $SrCO_3$, MnO_2, and TiO_2 (purity ⩾ 99.0%, Aladdin, Co., Ltd., China) were used as raw materials. These raw materials were mixed according to the stoichiometric ratios and ball milled at 250 rpm for 24 h in a planetary miller using ZrO_2 balls and ethanol as the medium. The milled slurry was dried at 65 ℃ for 12 h. Then the dry ceramic powders were ground, sieved, and calcined at 1300 ℃ for 4 h to form BSMT perovskite crystallites. After mixing with 5 wt% polyvinyl butyral, the BSMT crystallite powders were axially pressed into pellets under 6 MPa and further isostatically pressed under 200 MPa. Finally, the ceramic plates were sintered in a temperature range of 1350–1450 ℃ and soaked for 0.5–3 h to obtain dense specimens. Both sides of specimens were polished and sputtered with a gold electrode for electric characterization.

2. 2 Characterization

X-ray diffraction (XRD) was used to determine the polycrystalline structure of BSMT ceramics using a Rigaku Ultima IV diffractometer with a Ni-filtered Cu Kα radiation (λ = 1.5406 Å) and a scanning step of 0.02°, from 20° to 80°. The data were further analyzed by the Rietveld refinement using Fullprof program. Hitachi S-3400N scanning electron microscope (SEM) with an energy dispersive X-ray spectroscopy (EDX) analysis was employed to observe the morphology and compositions of BSMT ceramic specimens. The relative density was calculated by the ratio of real density measured using the Archimedes' method and the theoretical density calculated based on XRD patterns. The permittivity as a function of frequency and temperature were obtained using the impendence analyzer (Agilent 4284A). The polarization–electric field (P–E) hysteresis loops as a function of electric field and temperature were procured using Saywer–Tower circuit (RADIANT Multiferroic Test System). The electrocaloric response in this study was directly obtained using a specially designed calorimeter, including a T-type thermocouple attached to the specimen and a high voltage signal amplifier as the power source. During the test, a step-like voltage was applied to the sample, and the voltage was maintained at a constant value for over 10 s to reach a thermal equilibrium with the surrounding. After that, the voltage was sharply reduced to zero. The typical thermal response time along the sample thickness direction is a few milliseconds. Moreover, a sharply withdrawing electric field was applied to eliminate the influence of joule heat generated in the sample. The detailed procedure can be found in our previous work [26].

3 Results and discussion

3. 1 XRD analyses

XRD patterns procured at room temperature for BSMT ceramics with x = 35, 40 mol% and y = 0, 0.1, 0.2, 0.3, 0.4, 0.5 mol% are presented in Figs. 1(a) and 1(b), which show that a pure perovskite structure without any impurity peaks detected, meaning no secondary phases are introduced by the incorporation of manganese ions in the $(BaSr)TiO_3$ (BST) ceramics. The Rietveld refinement carried out for all the XRD patterns has given a reasonable fit of XRD diffraction (R_{wp} ⩽ 10.00%). A single (200) diffraction peak, instead of split double peaks near 45° confirms that the pseudo-cubic structures with a $Pm3m$ point group were present for all the compositions at room temperature. In view of our previous work and other publications reported for manganese ions doped $Ba(ZrTi)O_3$ ceramics, manganese ions were confirmed as Mn^{2+} ions using the X-ray photoelectronic spectroscopy [19,27,28]. Furthermore, the replacement of Sr^{2+} ions to metal ions at A-sites of ABO_3 perovskite structure in BSMT ceramics leads to a lattice distortion and even to a structural/compositional fluctuation for large Sr^{2+} ionic contents, forming a BST relaxor ferroelectric. Consequently, the relaxor ferroelectric behaviors will play a major role in both the structural and electrical properties in BSMT ceramics with the large Sr^{2+} contents.

3. 2 SEM results and microstructural analysis

Figure 2 shows the SEM images of BSMT specimens with x = 35, 40 mol% and y = 0, 0.1, 0.2, 0.3, 0.4, 0.5 mol%. As shown in Fig. 2, dense and uniform ceramics with distinct grain boundaries and 1–7 μm in grain sizes and over 97% of relative densities indicate that dense ceramics are formed during the sintering process. Furthermore, EDX mapping of Mn^{2+} ionic distribution shown in Fig. 3 implies that when the doped Mn^{2+} ions are in low content, a small portion of Mn^{2+} ions will enter into the ceramic grains and the others are probably to be distributed along the grain boundaries, which can be verified by the shift of XRD peaks and

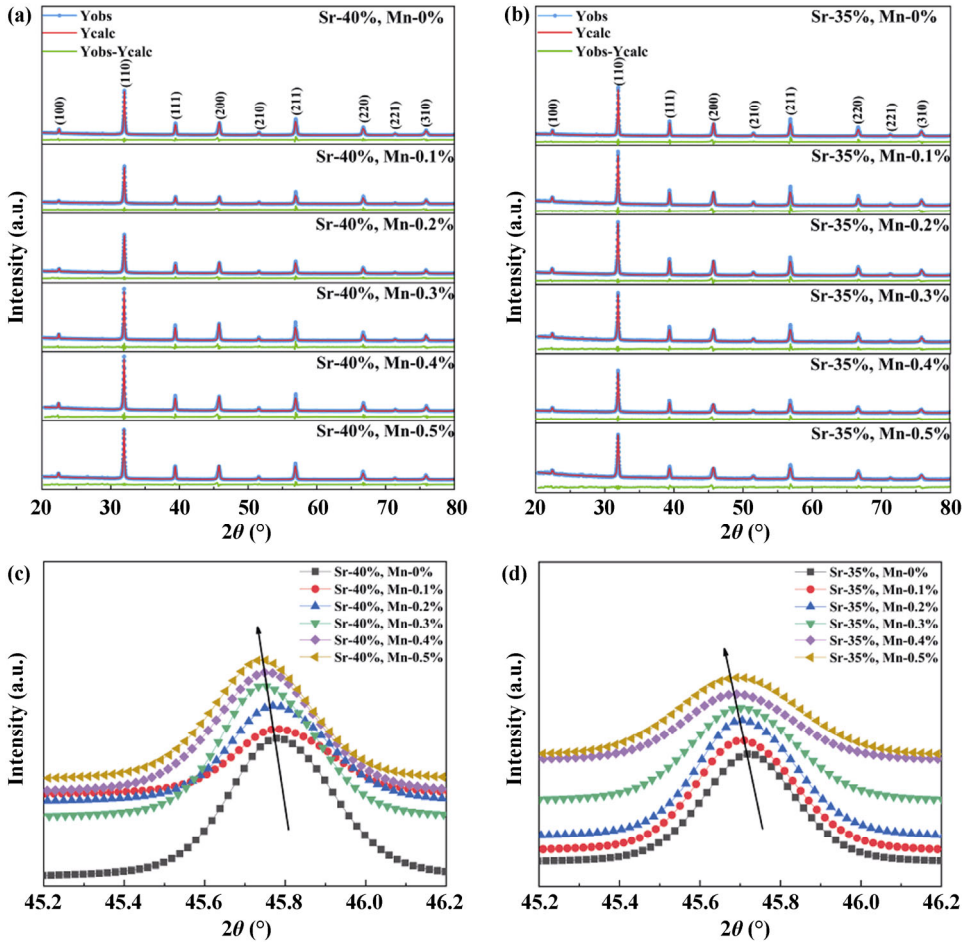

Fig. 1 (a, b) XRD patterns and Rietveld refinement and (c, d) magnified patterns for BSMT ceramics with (a, c) x = 40 mol%, y = 0, 0.1, 0.2, 0.3, 0.4, 0.5 mol% and (b, d) x = 35 mol%, y = 0, 0.1, 0.2, 0.3, 0.4, 0.5 mol% at room temperature.

the peak of permittivity as a function of temperature when the Mn^{2+} ions are introduced.

3. 3 Dielectric properties

The permittivity and dielectric loss as a function of temperature and frequency for BSMT ceramics with Sr^{2+} content of 40 mol% are plotted in Fig. 4(a), while the dielectric properties for BSMT ceramics with Sr^{2+} content of 35 mol% are plotted in Fig. 4(b). As shown in Figs. 4(a) and 4(b), the ferroelectric–paraelectric phase transition temperature shifts towards low temperatures with the increasing Sr^{2+} content, i.e., from 23.9 ℃ for BSMT–Sr^{2+} 35 mol%, Mn^{2+} 0 mol% to 14.3 ℃ for BSMT–Sr^{2+} 40 mol%, Mn^{2+} 0 mol%, resulting from the compositional fluctuation introduced by the doping of Sr^{2+} ions. Similarly, the impact of Mn^{2+} ions on the transition temperature is close to the Sr^{2+} ions. However, there is almost no shift for 0.1 mol% of $Mn^{2+}$and 35 mol% of Sr^{2+}, but a significant shift can be observed for 0.1 mol% of $Mn^{2+}$and 40 mol% of Sr^{2+}. For other Mn^{2+} contents, the shifts are usually larger for BSMT–Sr^{2+} 40 mol% than for BSMT–Sr^{2+} 35 mol%. In addition, it is observed that the permittivity peak moves towards high temperatures with the increasing frequency, indicating a relaxor ferroelectric characteristic. This is due to the large Sr^{2+} ionic content in the BSMT ceramics. It is also noted that, with the increasing manganese ionic content, the permittivity of BSMT specimens increases first and then declines for both the ceramics (35 and 40 mol% of Sr^{2+}). It means that in the course of incorporation of Mn^{2+} ions, Mn^{2+} ions enter into the lattice, and change the polar states in the ceramics, especially the nanosized polar domains in the relaxor ferroelectric ceramics, which may lead to the enhancement of permittivity near the phase transition [29]. The maximum value of relative dielectric constant of 23,171 is obtained in $(Ba_{0.6}Sr_{0.4})(Mn_{0.001}Ti_{0.999})O_3$ sample with a loss tangent of 0.9% at T_c = 9.5 ℃ and 1 kHz. It can also be noted that, as the Mn^{2+} ionic content increases, the largest loss tangent in the temperature

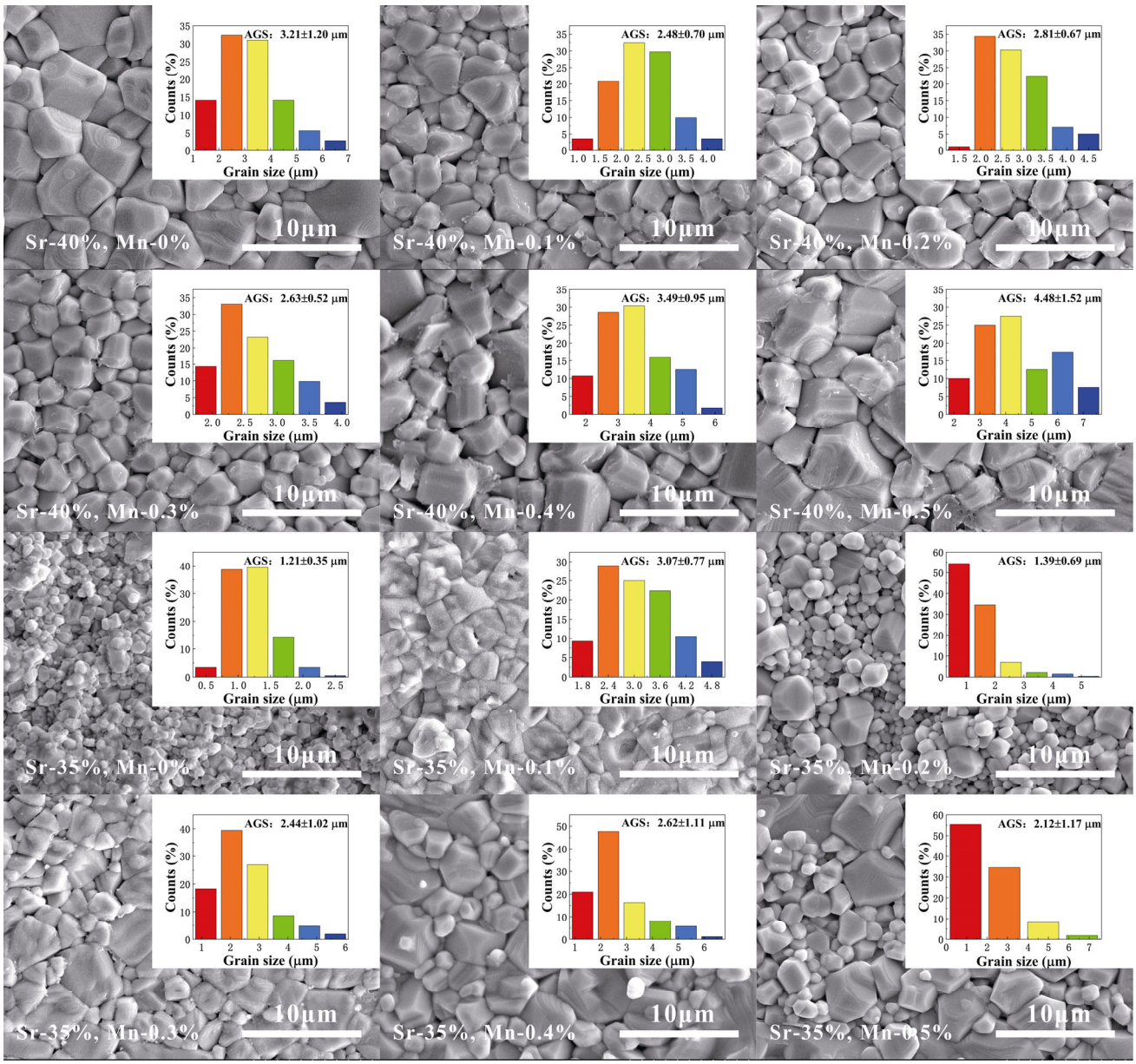

Fig. 2 SEM of BSMT ceramics with x = 35, 40 mol% and y = 0, 0.1, 0.2, 0.3, 0.4, 0.5 mol%. The inset of each panel shows the statistics of grain size distribution.

range of (–20)–110 ℃ for all 35 mol% of Sr^{2+} doped BSMT decreases (from 5%@Mn^{2+} 0 mol%, 1 kHz to 1%@Mn^{2+} 0.1 mol%, 1 kHz), and then increases, which implies that a relatively low manganese ionic content (less than 0.4 mol%) can enhance the permittivity. The reason is probably due to the acceptor-type compensation of Mn^{2+} ions with oxygen vacancies, i.e., during the sintering process at high temperatures, Mn^{4+} in raw material (MnO_2) will release two electrons to compensate the oxygen vacancies and to lead to the mitigation of the concentration of oxygen vacancies, thus reducing the loss tangent in the specimens.

3.4 *P–E* hysteresis loop

Polarization as a function of applied electric field for BSMT ceramics measured at –20 ℃, 100 ℃, and room temperature and 100 Hz under an external electric field of 50 kV/cm is shown in Fig. 5. The *P–E* loops of all compositions of BSMT show typical hysteresis loops of relaxor ferroelectrics which become slimmer with the increasing Mn^{2+} content at –20 ℃. The remnant polarization reduces from 6.26 μC/cm^2 for $(Ba_{0.65}Sr_{0.35})TiO_3$ to 2.45 μC/cm^2 for $(Ba_{0.65}Sr_{0.35})(Mn_{0.005}Ti_{0.995})O_3$, and from 6.11 μC/cm^2 for $(Ba_{0.6}Sr_{0.4})TiO_3$ to 2.20 μC/cm^2 for $(Ba_{0.6}Sr_{0.4})(Mn_{0.005}Ti_{0.995})O_3$, indicating a typical

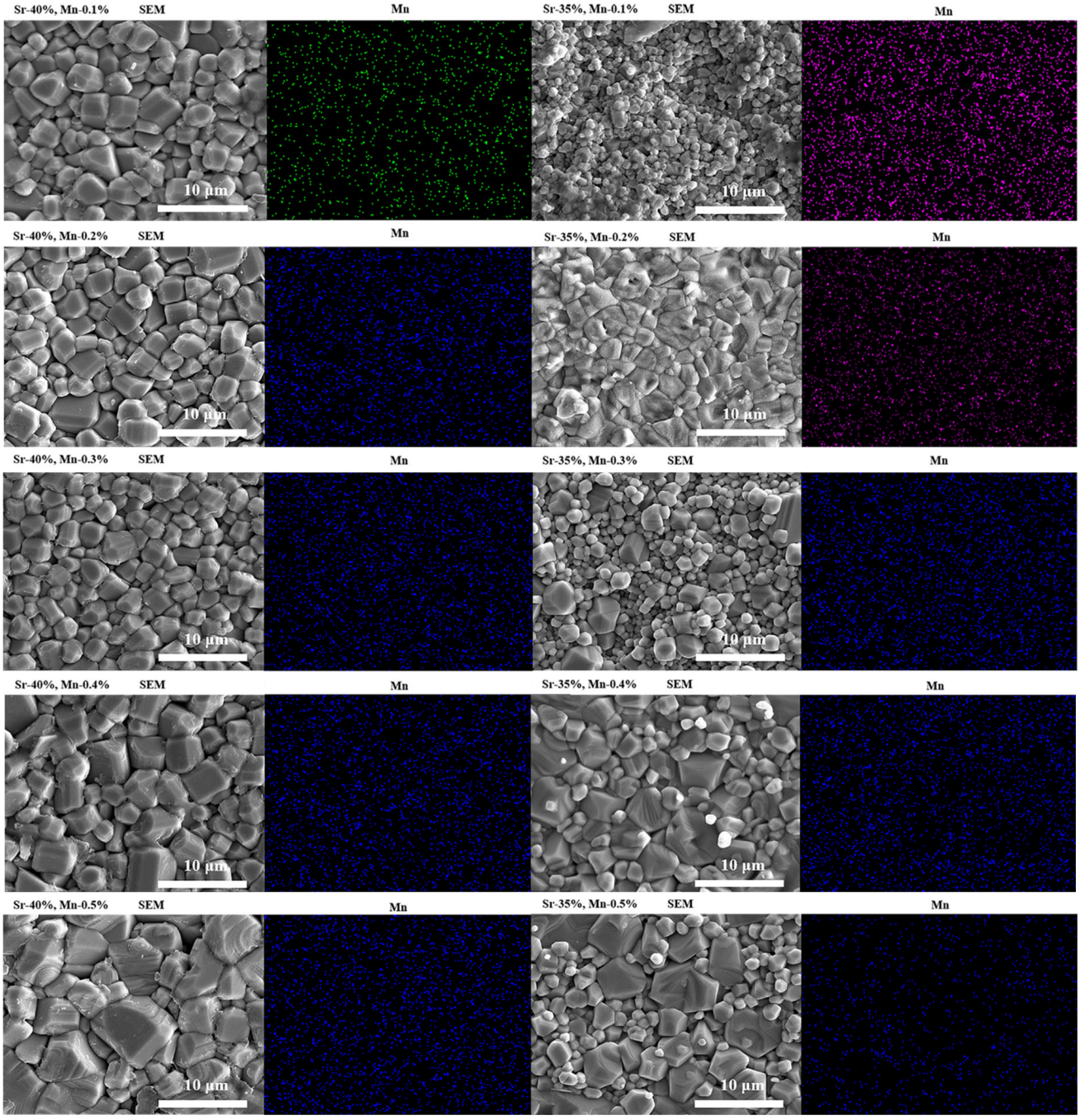

Fig. 3 EDX-mapping for Mn^{2+} distribution in BSMT ceramics with x = 35, 40 mol% and y = 0, 0.1, 0.2, 0.3, 0.4, 0.5 mol%.

hysteresis loop for relaxor ferroelectrics with nanometer sized domains. This phenomenon further indicates that the incorporated Mn^{2+} ions reduce the electric domains and make the permittivity increased. In addition, the maximum saturation polarization of 21.67 μC/cm^2 is procured for $(Ba_{0.65}Sr_{0.35})(Mn_{0.002}Ti_{0.998})O_3$ sample at –20 ℃ and 50 kV/cm. The saturation polarization increases first and then reduces with the increasing Mn^{2+} ionic content of BSMT (35 and 40 mol% of Sr^{2+}), which shows the similar tendency as the dielectric properties as a function of Mn^{2+} content.

3. 5 ECE

ECE is defined as the isothermal entropy change and ΔT in polar materials when an external electric field is applied or removed. When the applied electric field is removed, the dipolar entropy of material increases in the adiabatic condition. In the meantime, the lattice

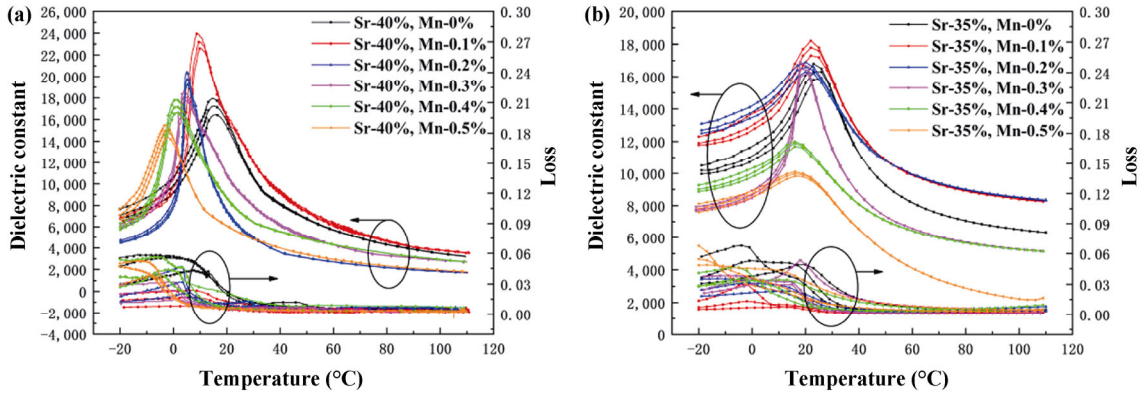

Fig. 4 Permittivity and loss tangent as a function of temperature for BSMT ceramics with x = (a) 40 mol% and (b) 35 mol%, and y = 0, 0.1, 0.2, 0.3, 0.4, 0.5 mol% measured at 100 Hz, 1 kHz, and 10 kHz.

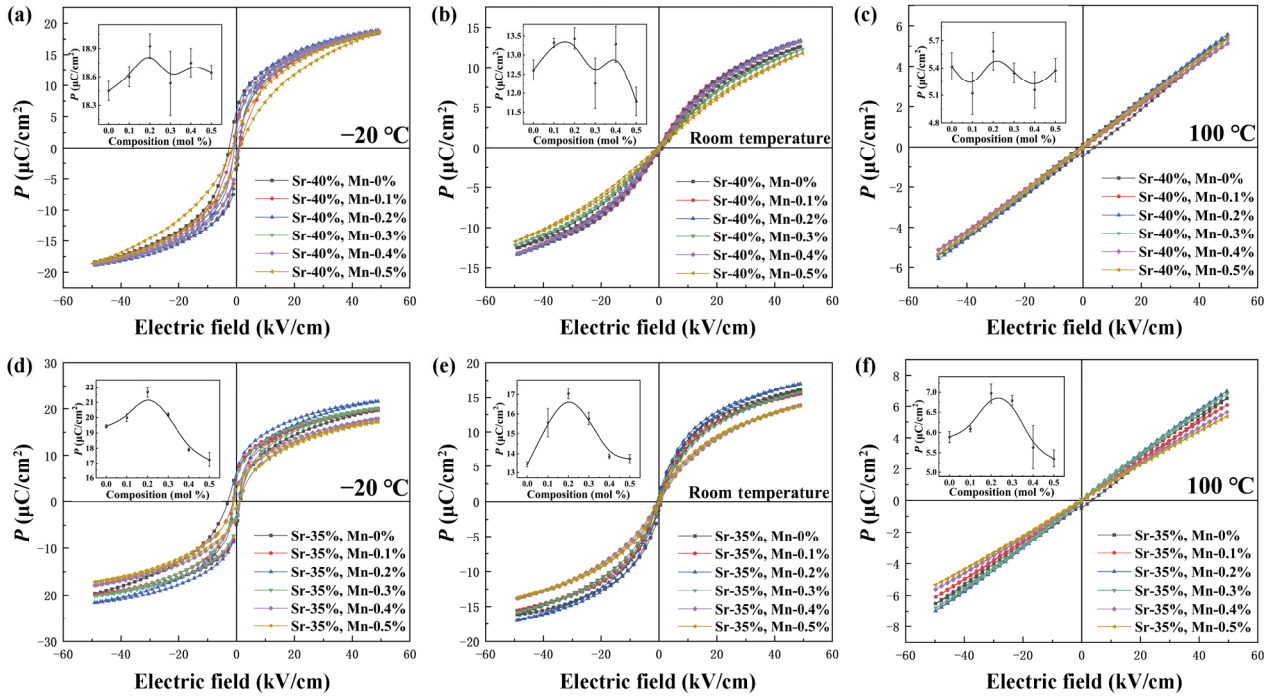

Fig. 5 P–E hysteresis loops for Mn^{2+} doped $(Ba_{0.6}Sr_{0.4})TiO_3$ (a–c) and $(Ba_{0.65}Sr_{0.35})TiO_3$ (d–f) ceramics measured at 5 MV/m and under –20 ℃, room temperature, and 100 ℃, respectively. The insets shows the saturation polarization as a function of Mn^{2+} content.

entropy decreases, resulting in the temperature drop of material since the total entropy of the material is kept as a constant. Here, except for the ΔS and ΔT, the electrocaloric strength $|\Delta T/\Delta E|$ is also used to estimate the ECE properties of the material.

For BSMT ceramics, the electrocaloric strength ($\mathrm{d}T/\mathrm{d}E$) can be calculated using the following equation [30]:

$$\frac{\mathrm{d}T}{\mathrm{d}E} = \frac{\beta \varepsilon_0 \varepsilon_r T P}{\rho C_v} \tag{2}$$

where ε_r is the relative dielectric constant (vacuum permittivity $\varepsilon_0 = 8.85 \times 10^{-12}$ F/m), T is the temperature, ρ is the density obtained by Archimedes' method, C_v is the specific heat capacity which is temperature depended. C_v as a function of temperature is presented in Fig. 6. Then calculated $\mathrm{d}T/\mathrm{d}E$ as a function of temperature is illustrated in Fig. 7, showing the obvious peaks of ECE strength near the T_c for all compositions. Comparing the directly measured $\mathrm{d}T/\mathrm{d}E$ with the calculated ones using Eq. (2), there is still a considerable space for improving the ECE performance.

The ΔT in this work was procured using a direct measurement. The measurement was pursued in the temperature ranging from –30 to 100 ℃ with an

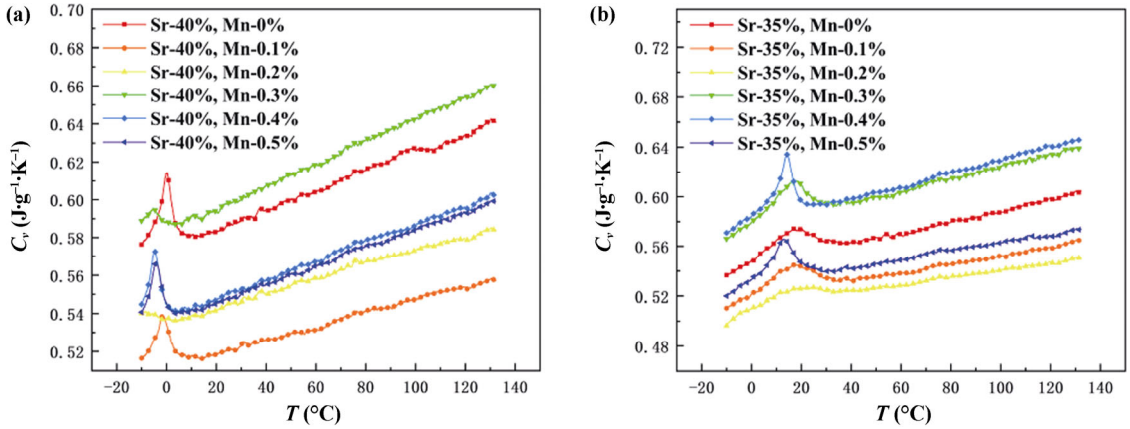

Fig. 6 Specific heat capacity as a function of temperature for manganese ion doped (a) $(Ba_{0.6}Sr_{0.4})TiO_3$ and (b) $(Ba_{0.65}Sr_{0.35})TiO_3$ ceramics.

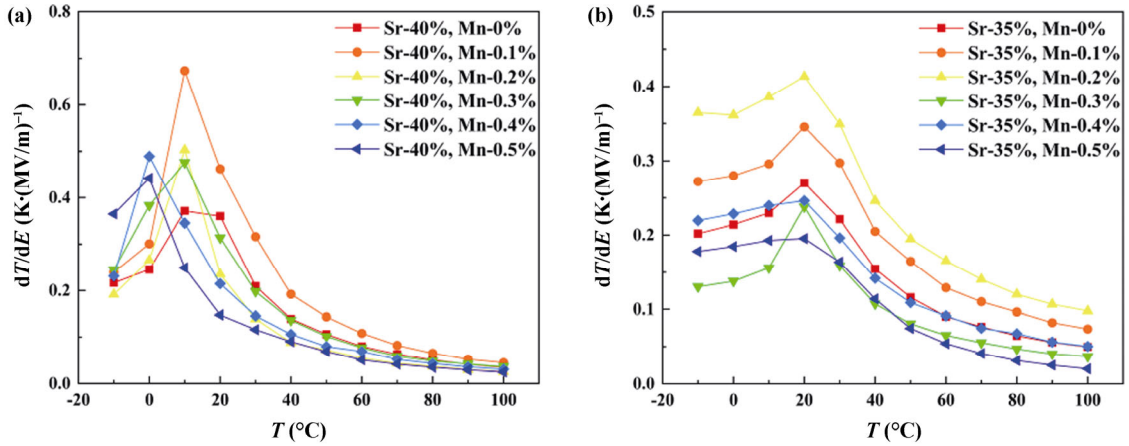

Fig. 7 Electrocaloric strength (dT/dE) as a function of temperature at 5 MV/m for Mn^{2+} doped (a) $(Ba_{0.6}Sr_{0.4})TiO_3$ and (b) $(Ba_{0.65}Sr_{0.35})TiO_3$ ceramics.

increment of 10 ℃ at 50 kV/cm and the results are shown in Figs. 8(a) and 8(b). The largest temperature change of 2.75 K with an ECE strength of 0.55 K·(MV/m)$^{-1}$ was obtained at ~21 ℃ and 50 kV/cm in $Ba_{0.6}Sr_{0.4}Mn_{0.001}Ti_{0.999}O_3$ sample. Moreover, $\Delta T > 2.2$ K at 5 MV/m over a wide temperature range of (–20)–100 ℃ was obtained in this sample, which is associated with the properties of a relaxor ferroelectric, in which the compositional and structural fluctuations probably expand T_c distribution of local nanometer sized domains, making the phase transition regime diffused [31]. Furthermore, for both 35 and 40 mol% Sr^{2+} doped BSMT specimens, the ΔT_{max} increases and then continuously decreases owing to the higher manganese ionic content resulting in reduction of polarization (Fig. 5). Especially, when a small number of manganese ions are doped in BSMT ceramics, the Mn^{2+} ions compensate the oxygen vacancies, reducing the loss tangent. When further increasing the manganese ionic concentration, the excess Mn^{2+} ions, behave as pinning centers for switchable domains and acceptor-type defect centers, leading to the mitigated polarization as well as ECE properties.

Various ECE materials have been widely investigated in recent years, including ferroelectrics, antiferroelectrics, and multiphase materials in the type of bulk, thin film, multilayer ceramic capacitors (MLCC) inorganic materials, and organic polymers, measured in either direct or indirect approaches [32–43]. Moreover, the ECE strength of 0.55 K·(MV/m)$^{-1}$ in this work is one of the highest values among the lead-free ferroelectric bulk ceramics published in recent years (Table 1). Obviously, low concentration of manganese doping can not only greatly enhance the permittivity, polarization, and ECE performance of BST ceramics, but also broaden the operational temperature range, demonstrating appropriate Mn^{2+} doping is an effective way for improving the ECE performance of ECE

materials. Based on the results, one can adjust the Mn^{2+} and Sr^{2+} ionic contents to obtain ferroelectric BSMT which is appropriate for ECE cooling devices, providing a promising ceramic system for ECE refrigeration devices.

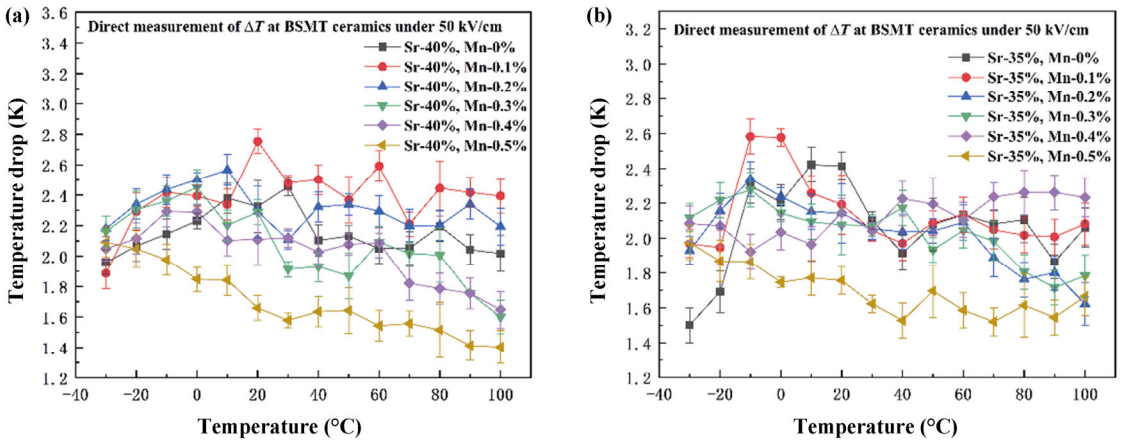

Fig. 8 ΔT for Mn^{2+} doped BST ceramics directly measured at temperature ranging from –30 to 100 ℃ under 5 MV/m: (a) Sr = 40% and (b) Sr = 35%.

Table 1 ΔT and electrocaloric strengths in various materials

Material	Form	T (℃)	ΔT (K)	ΔE (MV/m)	$\lvert\Delta T/\Delta E\rvert$ (K·(MV/m)$^{-1}$)	Method	Ref.
$Ba_{0.6}Sr_{0.4}TiO_3$	Bulk	30	2.46	5	0.49	Direct	This work
$Ba_{0.6}Sr_{0.4}Mn_{0.001}Ti_{0.999}O_3$	Bulk	21	2.75	5	0.55	Direct	This work
$Ba_{0.6}Sr_{0.4}Mn_{0.002}Ti_{0.998}O_3$	Bulk	10	2.57	5	0.51	Direct	This work
$Ba_{0.6}Sr_{0.4}Mn_{0.003}Ti_{0.997}O_3$	Bulk	0	2.45	5	0.49	Direct	This work
$Ba_{0.6}Sr_{0.4}Mn_{0.004}Ti_{0.996}O_3$	Bulk	–10	2.29	5	0.46	Direct	This work
$Ba_{0.6}Sr_{0.4}Mn_{0.005}Ti_{0.995}O_3$	Bulk	–30	2.09	5	0.42	Direct	This work
$Ba_{0.65}Sr_{0.35}TiO_3$	Bulk	10	2.42	5	0.48	Direct	This work
$Ba_{0.65}Sr_{0.35}Mn_{0.001}Ti_{0.999}O_3$	Bulk	–10	2.58	5	0.52	Direct	This work
$Ba_{0.65}Sr_{0.35}Mn_{0.002}Ti_{0.998}O_3$	Bulk	–10	2.34	5	0.47	Direct	This work
$Ba_{0.65}Sr_{0.35}Mn_{0.003}Ti_{0.997}O_3$	Bulk	–10	2.28	5	0.46	Direct	This work
$Ba_{0.65}Sr_{0.35}Mn_{0.004}Ti_{0.996}O_3$	Bulk	80	2.26	5	0.45	Direct	This work
$Ba_{0.65}Sr_{0.35}Mn_{0.005}Ti_{0.995}O_3$	Bulk	–30	1.98	5	0.40	Direct	This work
$Ba(Sn_{0.11}Ti_{0.89})O_3$	Bulk	44	0.63	2	0.315	Direct	[22]
$Ba_{0.8}Zr_{0.2}TiO_3$	Bulk	39	4.5	14.5	0.31	Direct	[30]
$Ba_{0.89}Hf_{0.11}TiO_3$	Bulk	70	0.35	1	0.35	Direct	[31]
$0.68Ba(Zr_{0.2}Ti_{0.8})O_3$–$0.32(Ba_{0.7}Ca_{0.3})TiO_3$	Bulk	63	0.33	2	0.17	Direct	[32]
$0.85K_{0.5}Na_{0.5}NbO_3$–$0.15SrTiO_3$	Bulk	67	1.9	15.9	0.12	Direct	[33]
$0.7Pb(Mg_{1/3}Nb_{2/3})O_3$–$0.3PbTiO_3$	Bulk	170	1.55	5	0.31	Direct	[34]
$PbZrO_3$	Bulk	97	–1.5	10	0.15	Direct	[35]
$Pb_{0.97}La_{0.02}(Zr_{0.80}Sn_{0.14}Ti_{0.06})O_3$	Bulk	50	–14.1	11	1.28	Indirect	[36]
$Ba_{0.7}Sr_{0.3}TiO_3$ MLCC	MLCC	40	4.8	50	0.10	Direct	[37]
Commercial $BaTiO_3$ MLCC	MLCC	130	13.94	68.52	0.20	Indirect	[38]
$0.65Pb(Mg_{1/3}Nb_{2/3})O_3$–$0.35PbTiO_3$	Thin film	154	2	8	0.25	Direct	[39]
$Pb_{0.8}Ba_{0.2}ZrO_3$	Thin film	17	45.3	59.8	0.76	Indirect	[40]
P(VDF–TrFE) 65/35 mol%	Polymer	50	35	180	0.22	Direct	[41]

4 Conclusions

In conclusion, BSMT ceramics with x = 35, 40 mol% and y = 0, 0.1, 0.2, 0.3, 0.4, 0.5 mol% were prepared using a conventional solid-state reaction approach. The permittivity and loss as a function of temperature and frequency show a high dielectric constant and low dielectric losses, obtaining in terms of adjusting the concentration of manganese ions from 0.1 to 0.4 mol%. In addition, polarization response is also enhanced by Mn^{2+} doping. Moreover, the maximal electrocaloric response of 2.75 K with electrocaloric strength of 0.55 K·(MV/m)$^{-1}$ was procured at ~21 ℃ and 50 kV/cm in $Ba_{0.6}Sr_{0.4}Mn_{0.001}Ti_{0.999}O_3$ sample. Furthermore, $\Delta T >$ 2.2 K at 5 MV/m over a broad temperature span of 120 ℃ was realized, which provides a promising candidate for practical ECE solid-state cooling devices.

Acknowledgements

This work was supported by the National Natural Science Foundation of China (Grant Nos. 51372042 and 51872053), the Guangdong Provincial Natural Science Foundation (Grant No. 2015A030308004), the NSFC–Guangdong Joint Fund (Grant No. U1501246), the Dongguan City Frontier Research Project (Grant No. 2019622101006), and the Advanced Energy Science and Technology Guangdong Provincial Laboratory Foshan Branch-Foshan Xianhu Laboratory Open Fund-Key Project (Grant No. XHT2020-011).

Electronic Supplementary Material

Supplementary material is available in the online version of this article at https://doi.org/10.1007/s40145-020-0450-1.

References

[1] Wang P, Bar-Cohen A. On-chip hot spot cooling using silicon thermoelectric microcoolers. *J Appl Phys* 2007, **102**: 034503.

[2] Fu Y, Nabiollahi N, Wang T, *et al*. A complete carbon-nanotube-based on-chip cooling solution with very high heat dissipation capacity. *Nanotechnology* 2012, **23**: 045304.

[3] Correia T, Zhang Q. *Electrocaloric Materials—New Generation of Coolers*. Berlin (Germany): Springer-Verlag Berlin Heidelberg, 2014.

[4] Lu SG, Zhang QM. Electrocaloric materials for solid-state refrigeration. *Adv Mater* 2009, **21**: 1983–1987.

[5] Valant M. Electrocaloric materials for future solid-state refrigeration technologies. *Prog Mater Sci* 2012, **57**: 980–1009.

[6] Wiseman GG, Kuebler JK. Electrocaloric effect in ferroelectric rochelle salt. *Phys Rev* 1963, **131**: 2023–2027.

[7] Mischenko AS, Zhang Q, Scott JF, *et al*. Giant electrocaloric effect in thin-film $PbZr_{0.95}Ti_{0.05}O_3$. *Science* 2006, **311**: 1270–1271.

[8] Neese B, Chu B, Lu SG, *et al*. Large electrocaloric effect in ferroelectric polymers near room temperature. *Science* 2008, **321**: 821–823.

[9] Lu SG, Rožič B, Zhang QM, *et al*. Organic and inorganic relaxor ferroelectrics with giant electrocaloric effect. *Appl Phys Lett* 2010, **97**: 162904.

[10] Rožič B, Kosec M, Uršič H, *et al*. Influence of the critical point on the electrocaloric response of relaxor ferroelectrics. *J Appl Phys* 2011, **110**: 064118.

[11] Plaznik U, Kitanovski A, Rožič B, *et al*. Bulk relaxor ferroelectric ceramics as a working body for an electrocaloric cooling device. *Appl Phys Lett* 2015, **106**: 043903.

[12] Sinyavsky YV, Brodyansky VM. Experimental testing of electrocaloric cooling with transparent ferroelectric ceramic as a working body. *Ferroelectrics* 1992, **131**: 321–325.

[13] Plaznik U, Vrabelj M, Kutnjak Z, *et al*. Electrocaloric cooling: The importance of electric-energy recovery and heat regeneration. *Europhys Lett* 2015, **111**: 57009.

[14] Ciomaga C, Viviani M, Buscaglia MT, *et al*. Preparation and characterisation of the $Ba(Zr,Ti)O_3$ ceramics with relaxor properties. *J Eur Ceram Soc* 2007, **27**: 4061–4064.

[15] Deluca M, Vasilescu CA, Ianculescu AC, *et al*. Investigation of the composition-dependent properties of $BaTi_{1-x}Zr_xO_3$ ceramics prepared by the modified Pechini method. *J Eur Ceram Soc* 2012, **32**: 3551–3566.

[16] Jian XD, Lu B, Li DD, *et al*. Direct measurement of large electrocaloric effect in Ba (Zr_xTi_{1-x}) O_3 ceramics. *ACS Appl Mater Inter* 2018, **10**: 4801–4807.

[17] Ma YB, Molin C, Shvartsman VV, *et al*. State transition and electrocaloric effect of $BaZr_xTi_{1-x}O_3$: Simulation and experiment. *J Appl Phys* 2017, **121**: 024103.

[18] Shukla A, Choudhary RNP, Thakur AK. Thermal, structural and complex impedance analysis of Mn^{4+} modified $BaTiO_3$ electroceramic. *J Phys Chem Solids* 2009, **70**: 1401–1407.

[19] Li HX, Jian XD, Niu X, *et al*. Direct measurement of enhanced electrocaloric effect in Mn^{2+} doped lead-free $Ba(ZrTi)O_3$ ceramics. *Scripta Mater* 2020, **176**: 67–72.

[20] Asbani B, Gagou Y, Trček M, *et al*. Dielectric permittivity enhancement and large electrocaloric effect in the lead free $(Ba_{0.8}Ca_{0.2})_{1-x}La_{2x/3}TiO_3$ ferroelectric ceramics. *J Alloys Compd* 2018, **730**: 501–508.

[21] Upadhyay SK, Fatima I, Reddy VR. Study of electrocaloric effect in Ca and Sn co-doped $BaTiO_3$ ceramics. *Mater Res Express* 2017, **4**: 046303.

[22] Sanlialp M, Luo Z, Shvartsman VV, *et al*. Direct measurement of electrocaloric effect in lead-free Ba $(Sn_xTi_{1-x})O_3$ ceramics. *Appl Phys Lett* 2017, **111**: 173903.

[23] Qi S, Zhang G, Duan L, *et al*. Electrocaloric effect in Pb-free Sr-doped $BaTi_{0.9}Sn_{0.1}O_3$ ceramics. *Mater Res Bull* 2017, **91**: 31–35.

[24] Luo ZD, Zhang DW, Liu Y, *et al*. Enhanced electrocaloric effect in lead-free $BaTi_{1-x}Sn_xO_3$ ceramics near room temperature. *Appl Phys Lett* 2014, **105**: 102904.

[25] Liu XQ, Chen TT, Wu YJ, *et al*. Enhanced electrocaloric effects in spark plasma-sintered $Ba_{0.65}Sr_{0.35}TiO_3$-based ceramics at room temperature. *J Am Ceram Soc* 2013, **96**: 1021–1023.

[26] Lu B, Yao YB, Jian XD, *et al*. Enhancement of the electrocaloric effect over a wide temperature range in PLZT ceramics by doping with Gd^{3+} and Sn^{4+} ions. *J Eur Ceram Soc* 2019, **39**: 1093–1102.

[27] Bao JB, Ren TL, Liu JS, *et al*. XPS Characterization on the Mn-doped BST thin films prepared by sol–gel method. *Integr Ferroelectr* 2002, **45**: 31–38.

[28] Shuai Y, Zhou S, Bürger D, *et al*. Decisive role of oxygen vacancy in ferroelectric versus ferromagnetic Mn-doped $BaTiO_3$ thin films. *J Appl Phys* 2011, **109**: 084105.

[29] Shvartsman VV, Kleemann W, Dec J, *et al*. Diffuse phase transition in $BaTi_{1-x}Sn_xO_3$ ceramics: An intermediate state between ferroelectric and relaxor behavior. *J Appl Phys* 2006, **99**: 124111.

[30] Lu SG, Li DD, Lin XW, *et al*. Influence of electric field on the phenomenological coefficient and electrocaloric strength in ferroelectrics. *Acta Phys Sin* 2020, **69**: 127701. (in Chinese)

[31] Smolensky GA. Physical phenomena in ferroelectrics with diffused phase transition. *J Phys Soc Jpn* 1970, **28**: 26–37.

[32] Qian XS, Ye HJ, Zhang YT, *et al*. Giant electrocaloric response over a broad temperature range in modified $BaTiO_3$ ceramics. *Adv Funct Mater* 2014, **24**: 1300–1305.

[33] Li JN, Zhang DW, Qin SQ, *et al*. Large room-temperature electrocaloric effect in lead-free $BaHf_xTi_{1-x}O_3$ ceramics under low electric field. *Acta Mater* 2016, **115**: 58–67.

[34] Sanlialp M, Shvartsman VV, Acosta M, *et al*. Electrocaloric effect in $Ba(Zr,Ti)O_3$–$(Ba,Ca)TiO_3$ ceramics measured directly. *J Am Ceram Soc* 2016, **99**: 4022–4030.

[35] Koruza J, Rožič B, Cordoyiannis G, *et al*. Large electrocaloric effect in lead-free $K_{0.5}Na_{0.5}NbO_3$–$SrTiO_3$ ceramics. *Appl Phys Lett* 2015, **106**: 202905.

[36] Peräntie J, Tailor HN, Hagberg J, *et al*. Electrocaloric properties in relaxor ferroelectric. $(1-x)Pb(Mg_{1/3}Nb_{2/3})O_{3-x}$ $PbTiO_3$ system. *J Appl Phys* 2013, **114**: 174105.

[37] Pirc R, Rožič B, Koruza J, *et al*. Negative electrocaloric effect in antiferroelectric $PbZrO_3$. *Europhys Lett* 2014, **107**: 17002.

[38] Zhuo F, Li Q, Gao J, *et al*. Giant negative electrocaloric effect in $(Pb,La)(Zr,Sn,Ti)O_3$ antiferroelectrics near room temperature. *ACS Appl Mater Inter* 2018, **10**: 11747–11755.

[39] Ding K, Zheng GP. Scaling for the refrigeration effects in lead-free barium titanate based ferroelectric ceramics. *J Electroceram* 2014, **32**: 169–174.

[40] Lu B, Wen XH, Tang ZH, *et al*. Large electrocaloric effect in $BaTiO_3$ based multilayer ceramic capacitors. *Sci China Technol Sc* 2016, **59**: 1054–1058. (in Chinese)

[41] Rožič B, Uršič H, Holc J, *et al*. Direct measurements of the electrocaloric effect in substrate-free PMN–0.35PT thick films on a platinum layer. *Integr Ferroelectr* 2012, **140**: 161–165.

[42] Peng BL, Fan HQ, Zhang Q. A giant electrocaloric effect in nanoscale antiferroelectric and ferroelectric phases coexisting in a relaxor $Pb_{0.8}Ba_{0.2}ZrO_3$ thin film at room temperature. *Adv Funct Mater* 2013, **23**: 2987–2992.

[43] Li XY, Qian XS, Gu HM, *et al*. Giant electrocaloric effect in ferroelectric poly(vinylidene fluoride-trifluoroethylene) copolymers near a first-order ferroelectric transition. *Appl Phys Lett* 2012, **101**: 132903.